

1 **Unveiling the anatomy of Termination 3 using water and air isotopes in the Dome C ice core, East**
2 **Antarctica**

3
4 Camille Bréant^{1,2}, Amaëlle Landais^{1,*}, Anaïs Orsi¹, Patricia Martinerie², Thomas Extier¹, Frédéric Prié¹,
5 Barbara Stenni³, Jean Jouzel¹, Valérie Masson-Delmotte¹ and Markus Leuenberger⁴

6
7 ¹ Laboratoire des Sciences du Climat et de l'Environnement, LSCE/IPSL, CEA-CNRS-UVSQ, Université
8 Paris-Saclay, Gif-sur-Yvette, France

9 ² Univ. Grenoble Alpes, CNRS, IRD, Grenoble INP, IGE, Grenoble, 38000, France

10 ³ Department of Environmental Sciences, Informatics and Statistics, University Ca' Foscari of Venice,
11 Venice, Italy

12 ⁴ Climate and Environmental Physics, Physics Institute and Oeschger Center for Climate Research,
13 University of Bern, Sidlerstrasse, 5, 3012 Bern, Switzerland

14
15 * corresponding author from February 2019: amaelle.landais@lsce.ipsl.fr

16
17
18

19 **Abstract**

20

21 Each glacial – interglacial transition of the Quaternary occurs in a different orbital context leading
22 to various timing for the deglaciation and sequence of high vs low latitudes events. Termination 3, 250
23 kiloyears before present (ka), is an unusual deglaciation in the context of the last 9 deglaciations
24 recorded in the old EPICA Dome C (EDC) Antarctic ice core: it exhibits a three-phase sequence, two
25 warming phases separated by a small cooling, the last phase suggesting a particularly rapid
26 temperature increase. We present here new high resolution $\delta^{15}\text{N}$ and deuterium excess (d-excess) data
27 from the EDC ice core to provide a detailed temperature change estimate during this termination.
28 Then, we combined the δD and $\delta^{18}\text{O}$ to discuss the relationship between high and low latitude changes
29 through the d-excess. We also provide the high vs low latitude sequence of events over this
30 deglaciation without chronological uncertainty using low latitude ice core proxies. In agreement with
31 previous studies based on speleothem analyses, we show that the first phase of Termination 3 (256 to
32 249 ka) is associated with small Heinrich like events linked to changes in ITCZ position, monsoon
33 activity and teleconnections with Antarctica. In a context of minimum Northern Hemisphere insolation,

34 this leads to a rather strong Antarctic warming, as observed in the $\delta^{15}\text{N}$ record in contrast to the
35 relatively small δD increase. The second warming phase occurs during the rise of the Northern
36 hemisphere insolation, with a large Heinrich like event leading to the characteristic Antarctic warming
37 observed in the $\delta^{15}\text{N}$ and δD increase as for the more recent terminations.

38

39 Keywords

40 Termination 3, deglaciations, ice core, water and air isotopes, Antarctic temperature, firn densification
41 model, bipolar seesaw, Heinrich like events

42

43

44 **1- Introduction**

45

46 The climate of the Quaternary is characterized by the succession of glacial and interglacial periods,
47 with a detailed description of their characteristics thanks to a diversity of proxy records from oceanic,
48 terrestrial and glacial archives, and dating methods (Spratt & Lisiecki 2016; Jouzel et al. 2007; Tzedakis
49 et al. 2017). The occurrence of glacial and interglacial periods is generally attributed to the driving
50 effect of changes in the seasonal and latitudinal distribution of incoming solar radiation, due to
51 changes in the Earth's astronomical characteristics (Milankovitch, 1941), as well as key Earth system
52 feedbacks, involving ice sheet and carbon cycle dynamics (Paillard & Parrenin 2004).

53 The exact mechanisms at play during glacial terminations remain however elusive, and
54 explanations for the timing of terminations, the different magnitudes of glacial-interglacial transitions,
55 and the interplay between multi-millennial trends and abrupt events are still incomplete. The accurate
56 documentation of multiple terminations, taking place under different orbital contexts, is one key line
57 of evidence (Yin and Berger, 2012; PAGES, 2016; Tzedakis et al., 2017). The important role of obliquity
58 is directly visible on the 40 kiloyears (hereafter ka) periodicity of glacial – interglacial cycles occurring
59 before the mid-Pleistocene transition and can also be dominant in the younger terminations (Huybers,
60 2007). In parallel, a recent study using East Asian speleothems showed that deglaciations of the last
61 650 ka occur every 4 or 5 precession cycles, confirming the important role of precession (Cheng et al.,

62 2016). The unfolding (or not) of a deglaciation during a precession cycle has been suggested to be
63 related to the glacial state, such as the initial ice volume (Paillard et al., 1998), or integrated summer
64 insolation (Tzedakis et al., 2017). The concentration of atmospheric greenhouse gases also plays a
65 major role during deglaciations. Several studies have shown, within age scale uncertainties, that
66 atmospheric CO₂ concentration and East Antarctic temperature started to increase synchronously at
67 the beginning of the last two deglaciations (Pedro et al., 2012; Landais et al., 2013; Parrenin et al.,
68 2013). The amplitude of simulated global temperature changes over deglaciations has been shown to
69 depend jointly on the amplitude of CO₂ concentration increase and insolation, namely obliquity for the
70 Southern Hemisphere and precession for the Northern Hemisphere (Yin and Berger, 2012).

71 The Antarctic EPICA Dome C (EDC) ice core provides very high resolution records encompassing
72 changes in local climate (with a resolution of 20 to 50 years back to 430 ka) as well as changes in
73 atmospheric composition and greenhouse gases concentrations of the last 9 terminations (EPICA
74 Community Members, 2004; Jouzel et al., 2007; Loulergue et al., 2008; Lüthi et al., 2008; Bereiter et
75 al., 2015). Together with the sea level record obtained from marine sediments (e.g. Röhlings et al., 2014;
76 Spratt and Lisiecki, 2016), the δD record from the EDC ice core shows that the last 5 terminations (i.e.
77 over the last 430 ka) are generally of higher amplitude than the terminations over the period 800 –
78 430 ka. Each termination still displays different characteristics (amplitude, rate of change) that were
79 discussed in previous studies (Röthlisberger et al., 2008; PAGES, 2016). In this context, Termination 3
80 seems associated with the most rapid temperature increase (increase of EDC δD at 14.8 ‰.ka⁻¹ for the
81 period 251.5 to 247.8 ka – Figure 1) making it a pertinent benchmark for the study of climate change
82 on relatively short timescales.

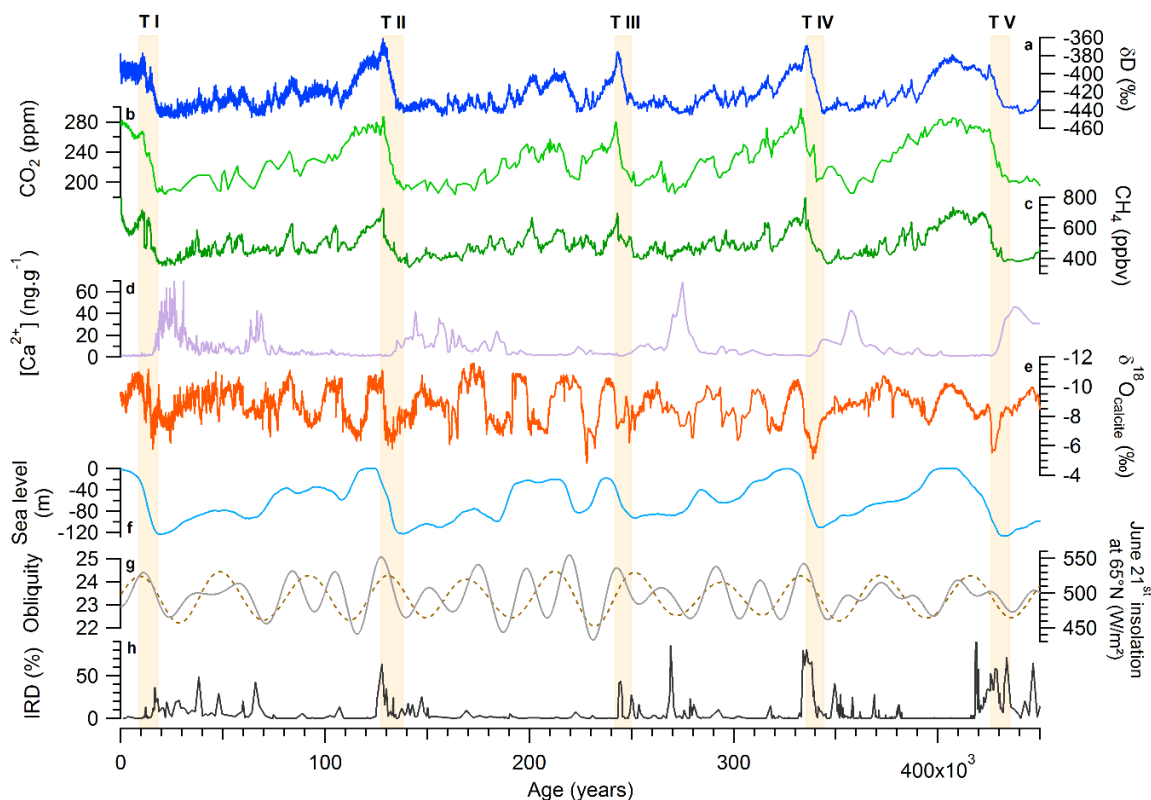
83 Marine records show that terminations of at least the last 500 ka are systematically associated
84 with the occurrence of iceberg discharges from the Laurentide ice sheet recorded as occurrence of
85 Heinrich like events in the IRD (Ice Rafted Debris characterized by a large amount of detrital quartz in
86 the sediment) in Atlantic marine cores (McManus et al., 1999; Hodell et al., 2008). In parallel, East
87 Asian speleothems highlight systematic Weak Monsoon Intervals (WMI) occurring during the

88 terminations synchronously with Heinrich like events and a rise in Northern Hemisphere summer
89 insolation (Cheng et al., 2009; 2016). Mechanistic links exist between Heinrich like events and WMI:
90 Heinrich like events are occurring over the same millennial periods as southward shifts of atmospheric
91 circulation in the Northern Hemisphere and in particular with southward shifts of tropical rain belts
92 (Chiang and Bitz, 2005). The Heinrich like events and associated lower latitudes climate changes are
93 hence fully embedded in the dynamic of terminations (e.g. Wolff et al., 2009; Denton et al., 2010).
94 Again, Termination 3 stands out being associated with 3 IRD peaks and 3 WMI while other terminations
95 over the last 450 ka are associated with only 1 or 2 IRD peaks (Jiang et al., 2010; Obrochta et al., 2014;
96 Figure 1). The unusual sequence observed over Termination 3 between millennial events and polar
97 temperature increase makes the study of Termination 3 key to understand the interactions between
98 millennial events (Heinrich Stadials, WMI) and orbital change (long term increase in CO₂ and polar
99 temperature).

100 Only few studies provided up to centennial resolution data for Termination 3, all of them
101 highlighting millennial scale variability during the end of marine isotopic stage 8 and Termination 3,
102 both in the Northern and in the Southern Hemispheres (i.e. between ~260 and 245 ka) (Pahnke et al.,
103 2003; Cheng et al., 2009; Jiang et al., 2010; Pérez-Mejías et al., 2017). In Antarctic deep ice cores, two
104 warming phases have been identified within Termination 3 (e.g. Watanabe et al., 2003; Röthlisberger
105 et al., 2008), the first one being associated with a relatively slow δD increase (5.18 ‰.ka⁻¹), interpreted
106 to reflect a gradual warming, before the fastest δD rise interpreted to reflect a fast warming.

107 Here, we focus on Termination 3 using new datasets from the EDC ice core. We combine water
108 isotopes (published δD and new $\delta^{18}O$ data) with new $\delta^{15}N$ of N₂ trapped in air bubbles, thereafter $\delta^{15}N$.
109 The combination of water isotopes, δD and $\delta^{18}O$ already published over the last 2 deglaciations at
110 Dome C (Stenni et al., 2001, 2010; Masson-Delmotte et al., 2010), can indeed be very useful to discuss
111 the relationship between local ($\delta^{18}O$ and δD at first order) and lower latitudes climatic changes
112 (deuterium excess or d-excess defined as $\delta D - 8 * \delta^{18}O$) (e.g. Vimeux et al., 1999; Uemura et al., 2018).
113 $\delta^{15}N$ is a proxy of firn processes driven by changes in local accumulation and temperature

114 (Severinghaus et al. 1998) providing an indicator of Antarctic climate change in the gas phase of the
 115 ice core records (Caillon et al., 2003; Landais et al., 2013). We briefly describe our methods, and discuss
 116 our results, including the reconstruction of site and source temperatures from water stable isotopes,
 117 and the drivers of $\delta^{15}\text{N}$ at EDC over Termination 3. We finally compare to previous records from other
 118 archives (marine sediment cores and speleothems) and discuss the sequence of events encompassing
 119 changes in Antarctic and global climate over Termination 3.



120

121 **Figure 1:** Climatic variations over the last 450 ka. a: δD record from EDC (Jouzel et al., 2007). b: Antarctic CO_2
 122 from EDC and Vostok (Lüthi et al., 2008). c: East Antarctic CH_4 record (Loulergue et al., 2008) d: Ca^{2+}
 123 concentration in the EDC ice core (Lambert et al., 2012). e: $\delta^{18}\text{O}_{\text{calcite}}$ from East Asian speleothems (Cheng et al.,
 124 2016). f: Global sea level change estimate (Bintanja et al., 2005). g: June 21st insolation at 65°N in solid line and
 125 obliquity in dotted line (Laskar et al., 2004). h: IRD percentage at site ODP980 (McManus et al., 1999). The timing
 126 of Termination 5 (TV) to Termination 1 (TI) is indicated by yellow bars. The 4 upper records are issued from the
 127 same ice core, hence with a maximum relative uncertainty of 1 ka on the chronology. On opposite, the 4 lower
 128 curves are all on their respective timescales (absolute timescale for obliquity and precession; timescale of each
 129 archive for the others) so that uncertainties of up to 6 ka can be attached to the comparison of the different
 130 records.

131

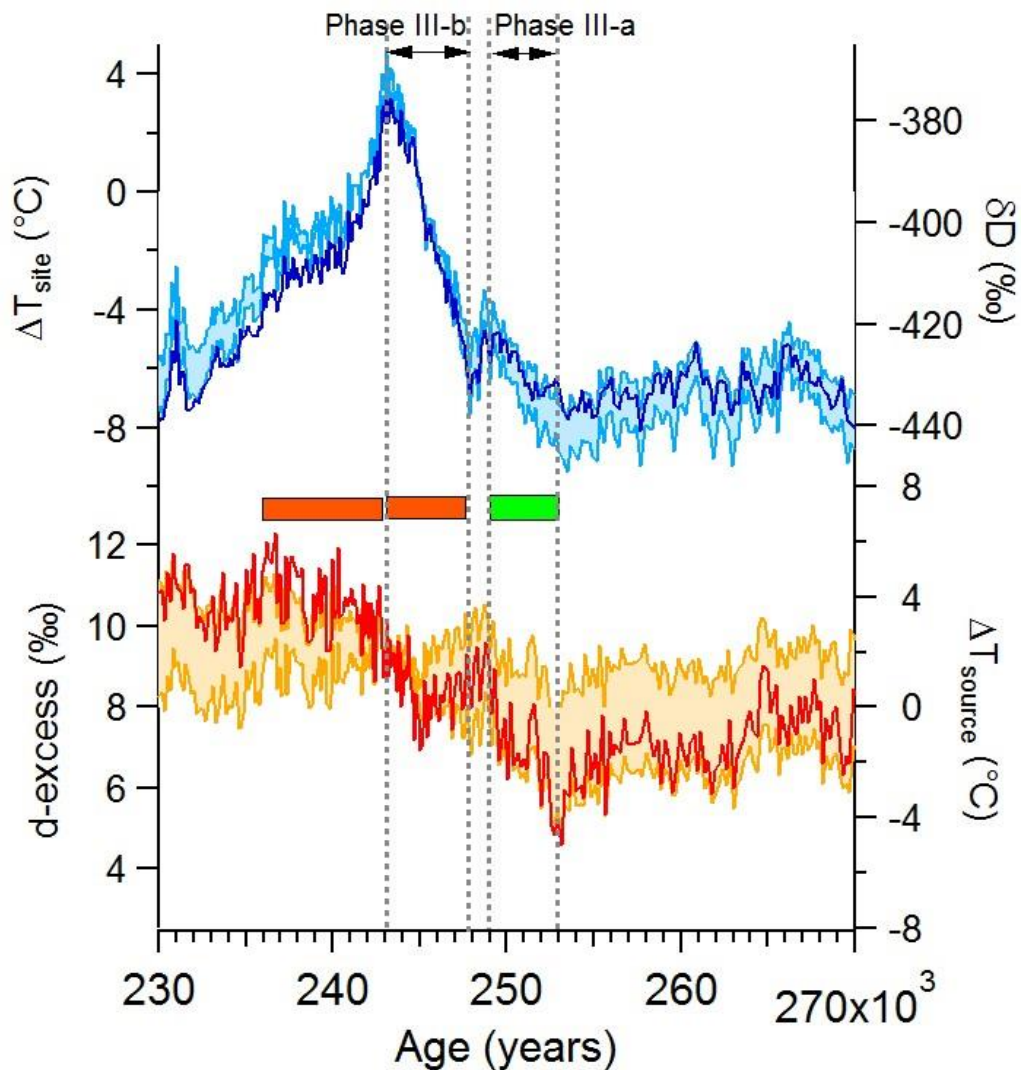
132 2- New data

133 2-1- EPICA Dome C (EDC) $\delta^{18}\text{O}$ and d-excess

134 Water $\delta^{18}\text{O}$ measurements of the Dome C ice core were performed along 55 cm samples at the
135 Department of Earth Sciences of University of Parma and at the Department of Geological,
136 Environmental and Marine Sciences of University of Trieste using a CO_2 / water equilibration method
137 (Meyer et al., 2000). These new measurements complete the 800 ka δD records of the EDC ice core
138 previously obtained at Laboratoire des Sciences du Climat et de l'Environnement and published in
139 (Jouzel et al., 2007). Home water standards were exchanged between the three institutes during the
140 measurement period to ensure the proper comparison of the δD and $\delta^{18}\text{O}$ data series. d-excess was
141 then calculated from the combined measurements of δD and $\delta^{18}\text{O}$ with a resulting accuracy of 1‰.

142 The δD and d-excess series presented on the section 3 cover the time period 230 to 270 ka with
143 an uncertainty of about 3 ka on the AICC2012 timescale (Bazin et al., 2013). This period corresponds
144 to the depth range 2232 to 2381 m and extends the EDC $\delta^{18}\text{O}$ and d-excess records over the last 140
145 ka (Stenni et al., 2010).

146 As already noted, the δD record shows a two-step increase for Termination 3: a first increase of
147 15‰ occurs from 253 to 249 ka (phase III-a, Figure 2). The same pattern was also observed on the
148 other deep ice cores covering Termination 3 on which water isotopes have been measured (SOM –
149 Figure S1). d-excess shows a parallel increase to δD over phase III-a. d-excess and δD are then anti-
150 correlated during the major δD increase of Termination 3 between 248 and 243 ka (phase III-b, Figure
151 2). Finally, d-excess reaches a maximum during the glacial inception, i.e. when δD is decreasing from
152 243 to 230 ka (Figure 2). This d-excess signal during glacial inceptions is a classical pattern also observed
153 for other glacial inceptions in Antarctic ice cores (Vimeux et al., 1999; Stenni et al., 2010; Uemura et
154 al., 2018): d-excess increases while δD decreases.



155

156 **Figure 2:** δD (in dark blue) and d -excess (in red) measurements on Dome C ice core with highlights on the phases
 157 of correlation (green rectangle) and anti-correlation (red rectangles) between these two proxies over the
 158 Termination 3. The ΔT_{site} and ΔT_{source} reconstructions within their uncertainty ranges are displayed in shaded
 159 areas. The vertical shaded lines display the limits of phase III-a and phase III-b.

160

161 **2-2- EDC $\delta^{15}N$**

162 Three series of measurements of $\delta^{15}N$ of N_2 have been performed along Termination 3 on the EDC
 163 ice core (Figure 3):

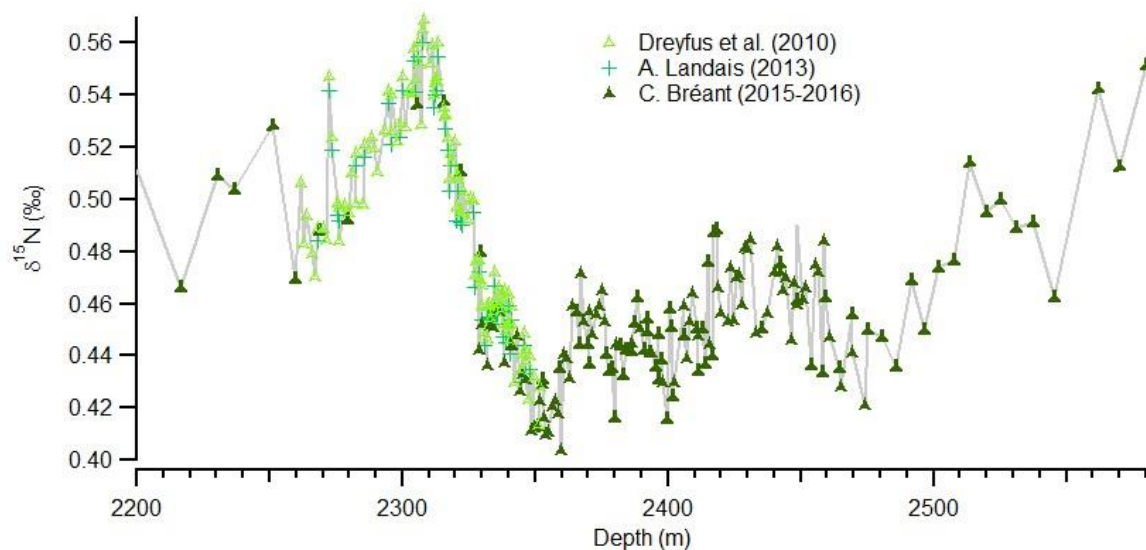
- 164 1- 50 duplicate samples (2262 to 2352 m depth) were measured in 2008 at Princeton University
 165 using a semi-automated wet extraction line with associated uncertainty of 7 ppm (Dreyfus et al.,
 166 2010).

167 2- 48 duplicate samples (2268 to 2348 m depth) were measured in 2013 at LSCE using a semi-
168 automated wet extraction line with associated uncertainty of 10 ppm (method in Capron et al.,
169 2010).

170 3- 172 duplicate samples (1904 to 2580 m depth) were measured in 2015-2016 at LSCE using the
171 same semi-automated wet extraction line and similar associated uncertainty of 10 ppm.

172 $\delta^{15}\text{N}$ measurements are expressed with respect to $\delta^{15}\text{N}$ of atmospheric air, with expected similar
173 values at Princeton University and at LSCE. Still, an average shift of + 0.007 ‰ has been found in the
174 original Princeton values compared to the LSCE data. The source of this offset is unknown. We thus
175 follow the correction of Dreyfus et al. (2010) and subtracted 0.007 ‰ from all Princeton data in the
176 set of data presented here.

177 As already shown in Dreyfus et al. (2010), $\delta^{15}\text{N}$ record shows a clear and strong increase from 2350
178 m to 2310 m depth probably corresponding to Termination 3 according to the AICC2012 gas age
179 timescale for EDC (Figure 3). After a $\delta^{15}\text{N}$ maximum at 2308 m probably associated with the end of
180 Termination 3, $\delta^{15}\text{N}$ shows a clear decrease from 2308 to 2250 m. Deeper in the core, the $\delta^{15}\text{N}$ record
181 is more scattered, showing a general decreasing tendency from 2580 m to 2350 m with some
182 fluctuations over the depth range 2480 m to 2350 m (Figure 3).



183
184 **Figure 3:** $\delta^{15}\text{N}$ data for Termination 3 of Dome C ice core using the correction for data measured in Princeton vs
185 LSCE proposed by Dreyfus et al. (2010).

186 The main $\delta^{15}\text{N}$ increase corresponding to Termination 3 on the EDC core was also observed on the
187 Vostok $\delta^{40}\text{Ar}$ data over the same termination (Caillon et al., 2003), $\delta^{40}\text{Ar}$ being assumed to be related
188 to physical fractionations in the firn before bubble enclosure as for $\delta^{15}\text{N}$ (see next section). Finally, $\delta^{15}\text{N}$
189 deglacial increase of $\sim 0.15\text{‰}$ was also clearly observed over the other terminations at EDC (Dreyfus et
190 al., 2010, SOM – Figures S2 and S3).

191

192 **3- Interpretation of the d-excess and $\delta^{15}\text{N}$ signals**

193 **3-1- Interpretation of water stable isotopes: site and source temperature**

194

195 Records of d-excess in Antarctic polar ice cores have classically been used to infer changes in
196 moisture sources / evaporation conditions following the studies of Vimeux et al. (1999), Stenni et al.
197 (2001), Vimeux et al. (2001), Masson-Delmotte et al. (2010), Markle et al. (2016) and Uemura et al.
198 (2018). In surface water vapour, at synoptic timescales, d-excess variations are mainly influenced by
199 variations in relative humidity controlling the relative influence of kinetic and equilibrium effects
200 (Merlivat and Jouzel, 1979; Gat et al., 1991). This influence is however muted when looking at the d-
201 excess evolution in polar regions and on longer timescales. Moreover d-excess is strongly modified
202 during distillation from the source to the polar precipitation regions through two effects: (1) the
203 dependence of equilibrium fractionation coefficient at condensation with temperature and (2) the
204 decrease of the slope δD vs $\delta^{18}\text{O}$ when both δD and $\delta^{18}\text{O}$ decrease toward very negative values (e.g.
205 Jouzel and Merlivat, 1984; Touzeau et al., 2016). This effect becomes predominant in very cold regions
206 of East Antarctica, for extremely low δD and $\delta^{18}\text{O}$. In these circumstances, local cooling leads to a d-
207 excess increase not linked to moisture source characteristics (Uemura et al., 2012). Alternative
208 definitions of d-excess using a logarithm formulation have thus been proposed to circumvent this site
209 temperature signal (e.g. Uemura et al., 2012; Markle et al., 2016; Dütsch et al., 2017). However, the
210 $\ln(\delta\text{D}+1)$ vs $\ln(\delta^{18}\text{O}+1)$ slope is not as constant as the $\delta^{18}\text{O}$ vs δD slope for large $\delta^{18}\text{O} - \delta\text{D}$ ranges, hence
211 leading to variable slope as a function of $\delta^{18}\text{O}$ values when defining the excess with a logarithm

212 definition. Here, we made the choice to show the d-excess curves keeping the classical d-excess
 213 definition. This choice of definition does not affect the reconstructions displayed below.

214 Following earlier studies of EDC d-excess, the combination of δD and d-excess can be used to
 215 reconstruct the local temperature (T_{site}) and the moisture source temperature (T_{source}). The moisture
 216 sources for precipitation at Dome C are located mainly in the temperate area of the Indian ocean
 217 (Masson-Delmotte et al., 2010). Here, we use the values for the T_{site} and T_{source} reconstructions for the
 218 EDC site given by Stenni et al. (2010) based on the use of a theoretical, mixed cloud isotopic model and
 219 the assumption that relative humidity is constant:

$$220 \quad \Delta T_{site} = 0.16 \times \Delta \delta D_{corr} + 0.44 \times \Delta d-excess_{corr} \quad (1)$$

$$221 \quad \Delta T_{source} = 0.06 \times \Delta \delta D_{corr} + 0.93 \times \Delta d-excess_{corr} \quad (2)$$

222
 223 The Δ symbol stands for the difference at each level between the measured or reconstructed
 224 parameter and the average of this parameter for the recent period (we performed the average over
 225 the last 2000 years for the reference to “the recent period”). $\Delta \delta D_{corr}$ and $\Delta d-excess_{corr}$ were
 226 calculated following Jouzel et al. (2003) using the $\delta^{18}O_{sea\ water}$ obtained in Bintanja et al. (2005)
 227 synchronized on EDC timescale (Parrenin et al., 2007):

$$228 \quad \delta D_{corr} = \left[\delta D - 8 \times \delta^{18}O_{sea\ water} \times \left(1 + \frac{\delta D}{1000} \right) \right] \div \left[1 + 8 \times \left(\frac{\delta^{18}O_{sea\ water}}{1000} \right) \right] \quad (3)$$

$$229 \quad \delta^{18}O_{corr} = \left[\delta^{18}O - \delta^{18}O_{sea\ water} \times \left(1 + \frac{\delta^{18}O}{1000} \right) \right] \div \left[1 + \left(\frac{\delta^{18}O_{sea\ water}}{1000} \right) \right] \quad (4)$$

$$230 \quad \Delta \delta D_{corr} = \delta D_{corr} - \delta D_{average} \quad (5)$$

$$231 \quad \Delta \delta^{18}O_{corr} = \delta^{18}O_{corr} - \delta^{18}O_{average} \quad (6)$$

$$232 \quad \Delta d - excess_{corr} = \Delta \delta D_{corr} - 8 \times \Delta \delta^{18}O_{corr} \quad (7)$$

233
 234
 235 These temperature reconstructions are based on the use of a mixed cloud isotopic model (Ciais and
 236 Jouzel, 1994) describing the evolution of water isotopic composition along a trajectory toward
 237 Antarctica and run over a large range of T_{site} and T_{source} . Different tunings of this model can however
 238 lead to significant variations in the coefficients of equations (1) and (2). Alternative reconstructions
 239

240 have thus been proposed (e.g. Uemura et al., 2012 for a complete study) enabling one to provide the
241 uncertainty range to the T_{site} and T_{source} reconstructions displayed on Figure 2. These alternative
242 reconstructions do not affect the shape of the reconstructed T_{site} and T_{source} variations but the
243 amplitudes of variations over Termination 3 are significantly affected, especially for the T_{source}
244 reconstruction (Figure 2).

245 The T_{site} and T_{source} reconstructions for Dome C are presented on Figure 2. While the evolution of
246 T_{site} is mainly parallel to the δD evolution and share many similarities with it, some differences are
247 observed. Over phase III-a, T_{site} displays an increase equivalent to 2/5 of the main T_{site} increase over
248 Termination 3 occurring during phase III-b. Over the same period (phase III-a, 253 to 249 ka), δD only
249 shows an increase of 1/4 of the main δD increase over phase III-b. The fact that the increase of EDC δD
250 over phase 1 of Termination 3 is relatively smaller than the corresponding T_{site} increase is probably
251 because δD is not only sensitive to the local temperature but rather to the temperature gradient
252 between the evaporative site and the precipitation site (i.e. between the first and final point of the
253 distillation trajectory). The T_{source} reconstruction based on d-excess data shows an increase over phase
254 III-a on Termination 3, in parallel to the T_{site} increase (Figure 2). Since both T_{site} and T_{source} increase by
255 similar amplitude, we expect that the result is the small δD signal observed on the EDC record. Over
256 phase III-b, T_{source} is not varying much (slight decrease) so that the dynamic of δD increase is directly
257 reflected in the T_{site} increase. T_{source} evolution is very different from the T_{site} evolution over glacial
258 inception: it follows the d-excess signal which remains at a relatively high level. This signal was already
259 largely discussed in Vimeux et al. (1999) and following studies: it reflects the fact that the temperature
260 of moisture source remains high during glacial inception favoring evaporation in temperate latitudes
261 and hence significant transport of moisture toward polar area to contribute to the growing of glacial
262 ice sheets.

263 The T_{site} and δD signals exhibit some differences during the glacial inception with the T_{site} signal
264 decreasing less rapidly than the δD signal. While this relatively slower decrease of T_{site} compared to δD
265 is also observed for other glacial inceptions and on the Vostok and Dome C ice cores (Vimeux et al.,

2001; Stenni et al., 2010; SOM – Figure S1), the differences in the T_{site} vs δD behaviours observed over Termination 3 is less obvious for the other terminations. Finally, note that the δD vs T_{site} differences are much less visible at the Dome F site, the δD signal at Dome F sharing more variability with the T_{site} signal than at Dome C or Vostok (SOM – Table T1).

270 **3-2- Interpretation of the $\delta^{15}\text{N}$ signal**

271
272 In a previous study (Bréant et al., 2017), we summarized the different possible influences on the
273 $\delta^{15}\text{N}$ in Antarctic ice core. $\delta^{15}\text{N}$ is directly related to the depth of the firn diffusive zone through
274 gravitational fractionation as $\delta^{15}\text{N}_{\text{grav}} = gz/RT$ at first order approximation with z the depth of the
275 diffusive zone, g the gravity acceleration constant, R the gas constant and T the mean temperature.
276 Note that a second order thermal effect is also expected in Antarctica when temperature gradients
277 occur in the firn following the equation $\delta^{15}\text{N}_{\text{therm}} = \Omega \times \Delta T$ with Ω the thermal fractionation coefficient
278 for stable isotopes of nitrogen (Grachev and Severinghaus, 2003) and ΔT the temperature gradient
279 between the top and the bottom of the firn. The depth of the firn diffusive zone is the difference
280 between the lock-in depth (LID) at the bottom of the firn and the depth of the convective zone at the
281 top of the firn. Previous studies based on dating constraints have shown that the existence of large
282 convective zones at Dome C during glacial periods is highly improbable (Parrenin et al., 2012; Bazin et
283 al., 2013; Veres et al., 2013) so that we concentrate here on the different influences on the firn LID.

284 The firn LID increases with increasing accumulation rate and decreases with increasing
285 temperature (increasing metamorphism speed). On the timescale of a deglaciation, both temperature
286 and accumulation increase so that LID is influenced by two opposite processes: LID decreases through
287 temperature increase and LID increases through accumulation increase. In addition, it has been
288 suggested that the concentration of impurities (taken into account through the Ca^{2+} concentration for
289 this purpose) can increase the densification speed in the firn (Hörhold et al., 2012; Freitag et al., 2013).
290 Since impurity concentration, as indicated by EDC calcium record (Röthlisberger et al., 2008),
291 systematically decreases during deglaciation, it should lead to an increase of LID and hence $\delta^{15}\text{N}$. While
292 these three effects can be accounted for in firn densification models (Freitag et al., 2013; Bréant et al.,

293 2017), reproducing the evolution of $\delta^{15}\text{N}$ over deglaciations in cold sites of East Antarctica with firn
294 densification models has long been a challenge (Sowers et al., 1992; Landais et al., 2006; Capron et al.,
295 2013; Bréant et al., 2017). In general, modeled $\delta^{15}\text{N}$ systematically decreases over terminations, while
296 ice core data indicate an increase of $\delta^{15}\text{N}$ during these periods. The temperature effect is thus
297 dominating the LID and $\delta^{15}\text{N}$ evolutions in the model at very cold sites, a feature which is not supported
298 by ice core records. In a recent firn model development (new IGE – previously LGGE – firn model), we
299 resolved the model-data mismatch by assuming that the creeping mechanism is different at very low
300 temperature (around -60°C) from the creeping mechanism at higher temperature (around -30°C)
301 (Bréant et al., 2017), a behavior supported by evidence from hot ceramic sintering (Wilkinson and
302 Ashby 1975; Bernache-Assolant, 2005).

303 Despite these firn model improvements, disentangling the effects of temperature, accumulation
304 rate and impurity concentration on the $\delta^{15}\text{N}$ evolution over deglaciations is challenging due to the
305 common co-variations of these parameters (SOM – Figure S2). Indeed, the reconstruction of snow
306 accumulation in ice cores from the East Antarctic plateau is based at first order on its relationship to
307 local temperature and inferred from water stable isotopic records (e.g. Parrenin et al., 2004). While
308 this assumption is challenged in coastal areas for centennial and millennial variability (e.g. Fudge et al.,
309 2016), the thermodynamic effect dominates at glacial to interglacial transitions. This reconstruction
310 can then be further refined using dated horizons and thinning scenarios from glaciological models as
311 done for example during the construction of the coherent ice core chronology AICC2012 (Bazin et al.,
312 2013; Veres et al., 2013). However, even with the constraints inferred from the dated horizons and
313 thinning scenarios, the accumulation rate increases significantly in parallel to δD and T_{site} over
314 deglaciations in Antarctica (SOM – Figure S2). In contrast, the link between temperature, accumulation
315 rate and Ca^{2+} is not always as strong. In particular, Termination 3 displays the strongest Ca^{2+}
316 concentration decrease observed 20 to 30 ka before the main accumulation rate and temperature
317 increase, themselves parallel to the δD signal (Figure 1, SOM – Figure S2). This makes Termination 3 a
318 unique deglaciation to disentangle the influences of impurity and temperature (accumulation).

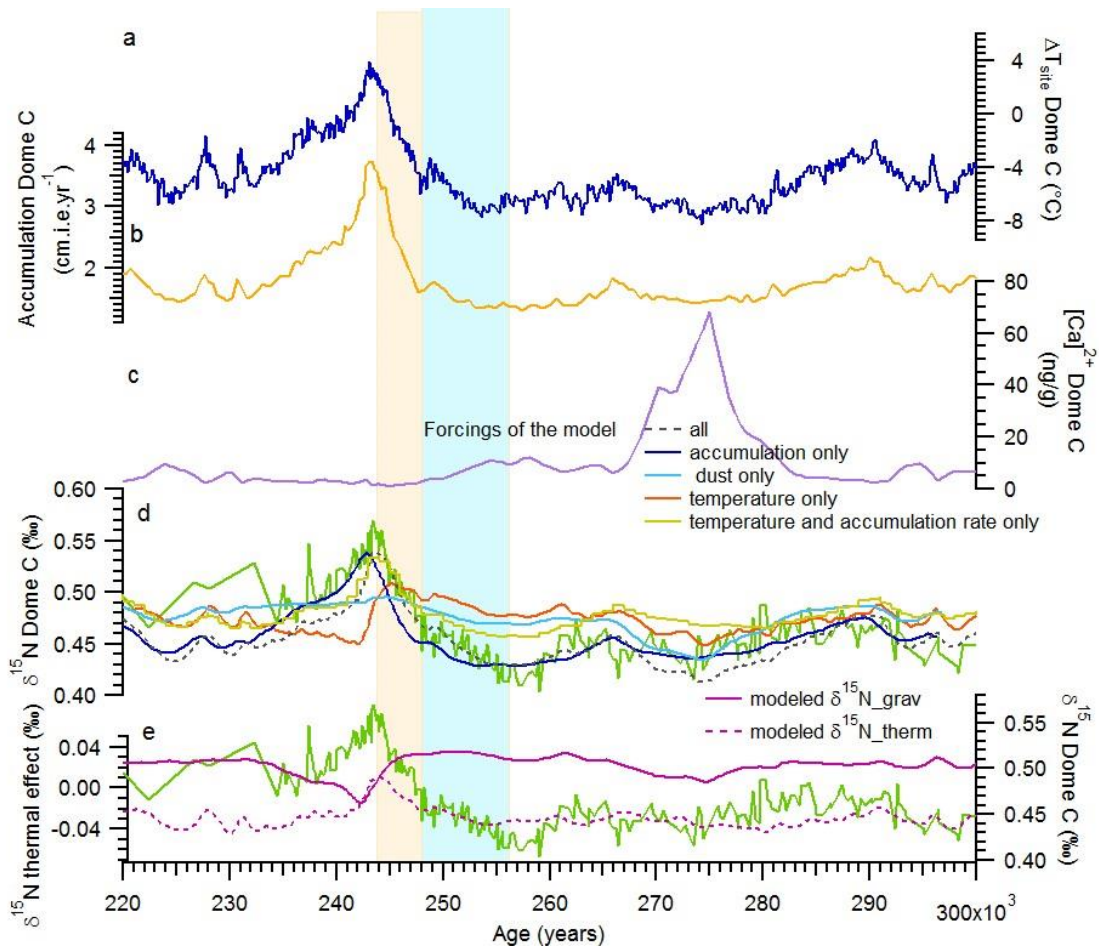
319 EDC $\delta^{15}\text{N}$ increase over Termination 3 is in two steps, the first one (+ 0.06 ‰) between 256 and
320 248 ka and the second one (+ 0.11 ‰) between 248 and 243 ka. These increases occur more than 15
321 ka later than the main impurity decrease, i.e. a temporal lag much larger than the maximum 1 ka
322 uncertainty in the relative chronology between gas age (on which $\delta^{15}\text{N}$ is displayed) and ice age (on
323 which Ca^{2+} and δD are displayed) (Bazin et al., 2013; Veres et al., 2013). Only a small decrease in $\delta^{15}\text{N}$
324 (less than 0.06 ‰) is observed around 270 ka corresponding to the major Ca^{2+} concentration peak
325 (Figure 4) with no significant changes in temperature and accumulation as inferred from the δD record.
326 All together, these observations suggest that impurity concentration is not the major driver of the $\delta^{15}\text{N}$
327 evolution over Termination 3.

328 In order to address this result more quantitatively, we have run the IGE firn densification model
329 equipped with impurity effect parameterization (Bréant et al., 2017) over the sequence of Termination
330 3 making the assumption that only impurity concentration is varying, hence keeping constant average
331 values for temperature and accumulation rate. At EDC where the $\delta^{15}\text{N}$ record is the longest, the model
332 produces a $\delta^{15}\text{N}$ decrease of 0.04 ‰ (compared to slightly less than 0.06 ‰ in the measurements) over
333 the major impurity concentration peak at 270 ka. Over the Termination 3 period where the main $\delta^{15}\text{N}$
334 increase is observed (256 to 244 ka), the model forced by impurity concentration only simulates a +
335 0.03‰ $\delta^{15}\text{N}$ increase while the measured $\delta^{15}\text{N}$ increases by 0.16‰ (Figure 4). The impurity effect is
336 hence not able to explain the $\delta^{15}\text{N}$ increase corresponding to Termination 3.

337 Most of the $\delta^{15}\text{N}$ increase over Termination 3 should thus be explained by changes in
338 accumulation rate and temperature. Increase in accumulation rate leads to increases in LID and then
339 in $\delta^{15}\text{N}$ through gravitational fractionation. At first order, the increase in $\delta^{15}\text{N}$ due to accumulation is
340 thus expected to be parallel with the increase in δD . To check such an hypothesis, we have simulated
341 the $\delta^{15}\text{N}$ evolution over the Termination 3 using the IGE firn densification model (Bréant et al., 2017)
342 forced by the AICC2012-derived accumulation rate only (i.e. with constant temperature and Ca^{2+}
343 concentration). A $\delta^{15}\text{N}$ increase of 0.103 ‰ is modelled between 253 and 243 ka (Figure 4). This change
344 is smaller but of the same order than the 0.16 ‰ increase of measured $\delta^{15}\text{N}$. However, the modeled

345 $\delta^{15}\text{N}$ is delayed by 2 ka compared to the measured $\delta^{15}\text{N}$. This shows that an additional effect also
346 influences the $\delta^{15}\text{N}$ signal.

347 The temperature effect is more complicated to infer than the accumulation rate effect. Indeed,
348 temperature can influence the $\delta^{15}\text{N}$ evolution either through the thermal effect or through the
349 gravitational effect because of a change of the LID induced by temperature variations. The
350 temperature increase during the deglaciation leads to a decrease of the LID because of increasing firn
351 metamorphism. This effect was dominating the modeled $\delta^{15}\text{N}$ evolution in cold sites in previous firn
352 densification models. However, this effect is muted in the new version of the IGE firn densification
353 model. Running this model over Termination 3 (Figure 4) with T_{site} forcing only leads to a $\delta^{15}\text{N}$ decrease
354 of 0.058‰ between 246 and 241 ka, this decrease integrating both the thermal and the gravitational
355 effects. The thermal effect leads to a slow increase of the modeled $\delta^{15}\text{N}$ between 256 ka and 244 ka
356 (total increase of 0.044‰, Figure 4). On opposite, the gravitational effect shows a mostly late decrease
357 of 0.05 ‰ between 246-241 ka, linked to the decrease of the firn depth. Combined to a thermal $\delta^{15}\text{N}$
358 decrease between 244 and 241 ka (Figure 4), it is responsible for the global modeled $\delta^{15}\text{N}$ decrease of
359 0.058‰ between 246 and 241 ka.



360

361 **Figure 2:** Comparison between EDC $\delta^{15}\text{N}$ data with $\delta^{15}\text{N}$ simulations run with the IGE firn densification model. a:
 362 scenario for temperature forcing (difference with present-day surface temperature). b: accumulation rate
 363 scenario (from AICC2012 – the modeled $\delta^{15}\text{N}$ is not significantly modified when using the accumulation rate
 364 reconstructed from water isotopes as in Parrenin et al., 2007). c: Ca^{2+} concentration used as input scenario for
 365 the firn densification model. d: comparison of measured (green) and modelled $\delta^{15}\text{N}$ for different configurations
 366 of the IGE firn densification model (all forcing in dark blue dashed line, only accumulation forcing in dark blue,
 367 only dust forcing in light blue, only temperature forcing in red, temperature and accumulation rate forcing in
 368 yellow). e: the purple lines on the lower panel show the outputs of the IGE model forced by temperature only for
 369 both its gravitational part (solid line, right y-axis) and its thermal part (dashed line, left y-axis). The blue rectangle
 370 indicates phase 1 and the yellow rectangle indicates phase 2.

371

372 Summarizing and based on our model-data comparison, we are now able to better explain the drivers

373 of the $\delta^{15}\text{N}$ increase over the two increasing phases of Termination 3 (blue and yellow bars on Figure 4).

374 During the first $\delta^{15}\text{N}$ increasing phase (blue on figure 4), the $\delta^{15}\text{N}$ increase is explained by a combination of
 375 thermal fractionation and accumulation effects, with a negligible contribution of impurity concentration.

376 During the second $\delta^{15}\text{N}$ increasing phase (yellow on figure 4), the $\delta^{15}\text{N}$ increase is essentially driven by the
 377 increasing accumulation rate, itself mainly related to increasing temperature. The direct temperature effect

378 plays a role in the early $\delta^{15}\text{N}$ increase over the second phase. However a few ka after the beginning of this

379 second $\delta^{15}\text{N}$ increasing phase, increasing thermal $\delta^{15}\text{N}$ and decreasing gravitational $\delta^{15}\text{N}$ effects
380 compensate each other so that the total effect is nil. When taking into account the influence of
381 temperature, accumulation rate and impurity concentration in the firn densification model as adjusted for
382 cold and low accumulation sites of East Antarctica (Bréant et al., 2017), we observe a total modeled $\delta^{15}\text{N}$
383 signal in very good agreement with our data for Dome C Termination 3 as was already observed for
384 Termination 1 (Bréant et al., 2017). This is an additional validation of the firn model development
385 performed by Bréant et al. (2017) since the phasing between changes in temperature and changes in
386 impurity concentrations is strongly different in Termination 1 and Termination 3. This good result can also
387 be extended to the whole 800 ka record (SOM – Figure S3).

388

389 **4- Discussion – East Antarctic climate dynamic over Termination 3**

390

391 One of the characteristics of Termination 3 on the EDC δD record is the succession of two
392 increasing phases (a first minor one followed by a larger one) between 253 and 244 ka with an
393 interruption at 248-249 ka. The existence of these two δD increasing phases are confirmed by the $\delta^{15}\text{N}$
394 measurements and T_{site} reconstruction. Indeed, the $\delta^{15}\text{N}$ increase over the first phase of Termination
395 3 at EDC is mainly influenced by local temperature and accumulation rate, itself partly related to
396 temperature through thermodynamic effects on multi-millennial timescale. The $\delta^{15}\text{N}$ and T_{site} data
397 hence show that the first phase of Termination 3 is of larger amplitude than suggested by the δD record
398 and probably started earlier (at 256 ka instead of 253 ka as suggested by the $\delta^{15}\text{N}$ signal).

399

400 **4-1- Specificity of Termination 3 in other climatic records**

401

402 This feature of Termination 3 is also strongly expressed in other records from relatively high
403 latitudes of the Southern Hemisphere, such as the $\delta^{18}\text{O}_{\text{planktonic}}$ record of Pahnke et al. (2003) in the
404 Southern Ocean, close to the east of New Zealand (Chatham Rise), reflecting either a local climatic and
405 hydrologic modification or a front shift during the first phase of Termination 3 (Figure 5). Note that this
406 record can be paralleled to the T_{source} reconstruction over the first phase of Termination 3 reflecting

407 either an increase of the oceanic temperature or a shift of the source evaporative region toward lower
408 latitudes.

409 In the Northern Hemisphere, several records highlighted a succession of millennial events
410 occurring prior to the main deglaciation signal of Termination 3 (Jiang et al., 2010; Obrochta et al.,
411 2014; Cheng et al., 2009, 2016; Pérez-Mejías et al., 2017). The fingerprints of Heinrich-like events have
412 been identified over this period (McManus et al., 2004), through cold periods in the Northern Atlantic
413 (Obrochta et al., 2014), dry events in Southern Europe (Pérez-Mejías et al., 2017) and WMI in East
414 Asian speleothems (Jiang et al., 2010; Cheng et al., 2009, 2016) (Figure 5). In particular, Cheng et al.
415 (2009) proposed a three-phase sequence of Termination 3, the first and last phases corresponding to
416 weak monsoon intervals. A parallel is proposed between the intermediate phase and the slight
417 Antarctic cooling between the two Antarctic warming phases III-a and III-b displayed on Figure 2. The
418 bipolar seesaw mechanism is expected to synchronize Greenland stadials with Southern ocean and
419 Antarctic warming (Blunier and Brook 2001; Stocker and Johnsen 2003; EPICA Community members,
420 2006; Barker et al., 2009; Landais et al., 2015; Pedro et al., 2018). Within the chronological
421 uncertainties of AICC2012 and age models of other archives (larger than 2 ka each), we follow Cheng
422 et al. (2009) and propose that the Antarctic warming during phase III-a of Termination 3 coincides with
423 the Heinrich-like event at 250 ka and WMI-III-a, and the Antarctic warming during phase III-b of
424 Termination 3 corresponds to the Heinrich like event at 245 ka and WMI-III-b. To keep coherency with
425 the notation first introduced by Cheng et al. (2009), we thus refer to T III-a and T III-b for the two
426 Antarctic warming phases over Termination 3, these warming phases corresponding very likely to WMI
427 III-a and WMI III-b.

428

429 **4-2- The sequence of Termination 3 on a coherent chronology using ice core proxies**

430

431 A way to circumvent the chronological issue between Antarctic records and lower latitude records
432 and to confirm the hypothesis proposed above and by Cheng et al. (2009) is to make a direct
433 comparison between the high latitude proxies ($\delta^{15}\text{N}$, T_{site} , δD) and low latitude proxies ($\delta^{18}\text{O}_{\text{atm}}$, CH_4 as

434 indirect tracers of the low latitude cycle, see below) all measured on the same EDC ice core. There is
435 thus no relative chronology uncertainty between the records except the maximum 1 ka uncertainty
436 (inferred from AICC2012) between records displayed on the gas timescale ($\delta^{15}\text{N}$, $\delta^{18}\text{O}_{\text{atm}}$, CH_4) and
437 those displayed on the ice timescale (δD , T_{site}). The $\delta^{18}\text{O}_{\text{atm}}$ signal shares many similarities with East
438 Asian $\delta^{18}\text{O}_{\text{calcite}}$ records at both orbital and millennial timescales (Wang et al., 2008; Severinghaus et
439 al., 2009; Extier et al., 2018) because it is directly influenced by the low latitude meteoric water $\delta^{18}\text{O}$
440 signal transmitted to the atmosphere through photosynthesis (e.g. Bender et al., 1994; Landais et al.,
441 2010; Seltzer et al., 2017). Moreover, Reutenauer et al. (2015) used a model approach to show that
442 Heinrich events are associated with synchronous millennial variability of both $\delta^{18}\text{O}_{\text{calcite}}$ in East Asia and
443 $\delta^{18}\text{O}_{\text{atm}}$. CH_4 can also provide information of low latitudes climate of the Northern Hemisphere since
444 the main CH_4 sources are located in wetlands of the low latitudes during glacial periods (Brook et al.,
445 2000). Still, high latitudes of the Northern Hemisphere may strongly contribute to the CH_4 atmospheric
446 signal especially when the high latitude continental areas are free of ice in warm periods (Yu et al.,
447 2013).

448 $\delta^{18}\text{O}_{\text{atm}}$ shows two increases over phases T III-a and T III-b (Figure 5). An interruption ($\delta^{18}\text{O}_{\text{atm}}$
449 decrease) is observed between the two phases, i.e. in phase with the slight decrease in T_{site} and $\delta^{15}\text{N}$.
450 This interruption at ~ 248 ka, also observed in the $\delta^{18}\text{O}_{\text{calcite}}$ and associated with the strengthening of
451 the East Asian Monsoon, could be linked to an Antarctic Cold Reversal as already observed over the
452 last deglaciation (Zhang et al., 2016) and suggested by Cheng et al. (2009). The correspondence
453 between $\delta^{15}\text{N}$ and $\delta^{18}\text{O}_{\text{atm}}$ is free from any chronological uncertainty since they are measured on
454 exactly the same air samples. This record hence supports a synchronicity between cold events in the
455 Northern Hemisphere (associated with Heinrich events and WMI) and warming in Antarctica over
456 phases T III-a and T III-b.

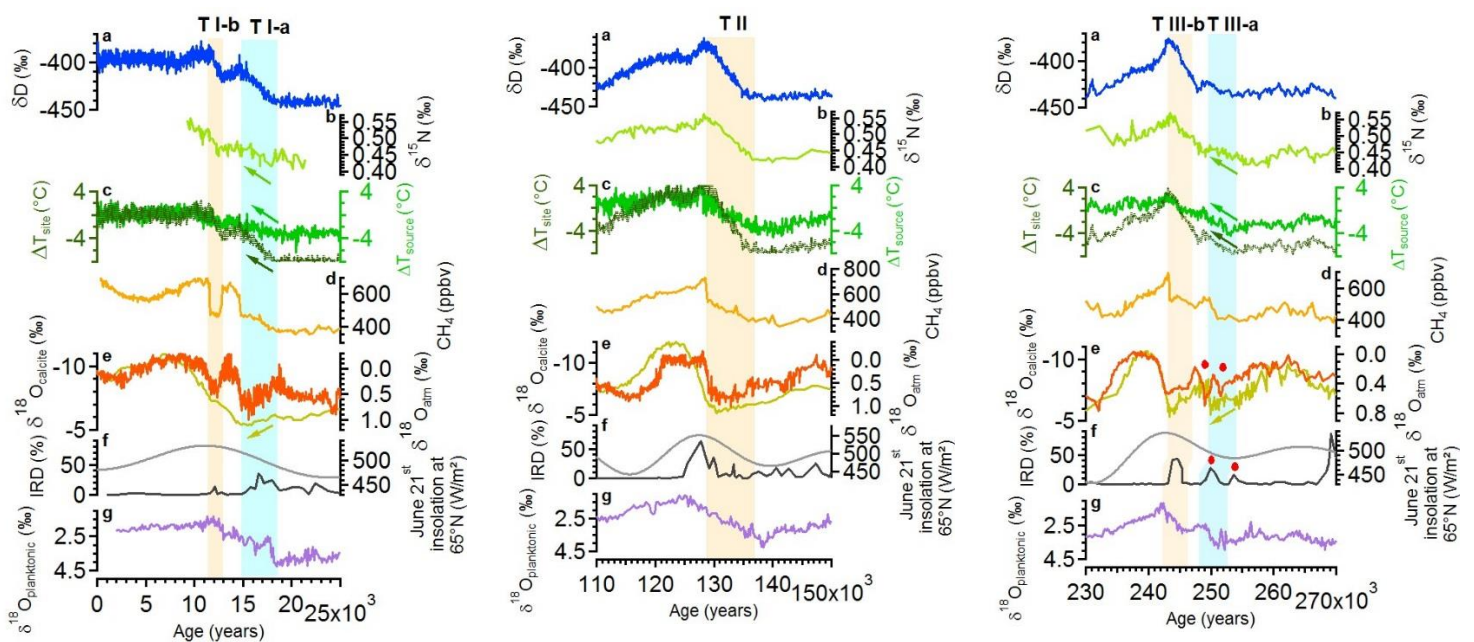
457 The CH_4 record is of relatively low resolution (400 years) and probably bears a significant influence
458 of the high latitude Northern Hemisphere during deglaciations. Still, it shows a clear increase over
459 phase T III-a peaking at 250 ka before a low level over phase T III-b. This increase is difficult to link to a

460 warming of the high latitudes since it corresponds to a minimum of summer insolation at 65°N (despite
461 high obliquity). Another possible interpretation of this signal is to link it to millennial-scale variability.
462 A previous study performed over the last climatic cycle and last deglaciation showed that a CH₄
463 increase of several tenths of ppb is observed at the time of iceberg discharge in the North Atlantic in
464 relationship with a shift of the tropical rain belts (Rhodes et al., 2015). The occurrence of a Heinrich
465 event and associated WMI over phase T III-a may hence explain this early CH₄ peak. The main increase
466 of CH₄ then occurs at the end of phase T III-b similarly to what is observed for the other deglaciations
467 (Figures 1 and 5).

468 Our new measurements hence permit to refine the sequence of events for Termination 3
469 including Antarctica without relative chronological uncertainty. During phase T III-a occurring during a
470 minimum of the summer insolation at 65°N, Heinrich like events are associated with a southward shift
471 of the Northern Hemisphere polar front and of the tropical rain belts linked with the ITCZ (Intertropical
472 Convergence Zone). This shift is observed in the increases of $\delta^{18}\text{O}_{\text{atm}}$, East Asia $\delta^{18}\text{O}_{\text{calcite}}$ and CH₄ and is
473 associated with the weak monsoon interval referred as WMI-III-a. Connected to this Northern
474 Hemisphere change through atmospheric and oceanic teleconnections linked to the bipolar seesaw,
475 the Antarctic temperature increases as shown by the T_{site} and $\delta^{15}\text{N}$ records. Despite evidences for the
476 Northern Hemisphere vs Antarctica correspondences, our records also show that the sub-millennial
477 variability recorded in the IRD and Chinese $\delta^{18}\text{O}_{\text{calcite}}$ records over phase T III-a (2 IRD peaks, 2 positive
478 $\delta^{18}\text{O}_{\text{calcite}}$ excursions, red points in Figure 5) is not seen in the Antarctic records which record only one
479 monotonous temperature increase.

480 Phase T III-b occurs during the rise of 65°N summer insolation and is characterized by a Heinrich
481 like event of larger amplitude, which is also associated with WMI III-b, a southward shift of the ITCZ
482 and of the Northern Hemisphere polar front. In a context of high Northern Hemisphere insolation and
483 similarly to other deglaciations in the same insolation context (e.g. the most recent and well dated
484 Terminations 1 and 2, cf Figure 1), the Antarctic temperature increases faster than during phase T III-
485 a.

486 Finally, the sequence of events over Termination 3 can be compared with the sequences observed
 487 on Termination 1 and Termination 2 where dating constraints are strong enough (Figure 5). In
 488 particular, Figure 5 shows that we systematically have parallel increase of $\delta^{15}\text{N}$, T_{site} and T_{source} at Dome
 489 C over the one or two Antarctic warming phases of the terminations. These warming phases are also
 490 systematically associated with IRD peaks as well as increasing phases in the $\delta^{18}\text{O}_{\text{calcite}}$ and $\delta^{18}\text{O}_{\text{atm}}$. The
 491 Antarctic warmings during the last 3 deglaciations are thus systematically correlated with the
 492 occurrence of WMI and iceberg discharges in the North Atlantic, hence a southward shift of the ITCZ.
 493 However, the peculiarity of Termination III is the fact that the warming over phase T III-a occurs during
 494 a minimum in June 21st insolation at 65°N while all Antarctic warming phases occur during a phase of
 495 increase in the June 21st insolation at 65°N. This may explain why phase T III-a is associated with a much
 496 smaller δD and T_{site} increase than phase T I-a. The occurrence of phase T III-a of Termination 3 in a
 497 context of low summer insolation at 65°N hence appears as an anomaly and suggests that other factors
 498 than the increase in summer insolation in the Northern Hemisphere may play a role in the triggering
 499 of the deglaciation in Antarctica. These factors may be local insolation (i.e. Southern Hemisphere
 500 summer insolation) or occurrence of millennial scale variability related to changes in the ITCZ locations.



501
 502 **Figure 5:** Millennial variability during the Terminations 1 (left), 2 (middle) and 3 (right). a: EDC δD record (Jouzel
 503 et al., 2007). b: measured EDC $\delta^{15}\text{N}$ (Dreyfus et al., 2010; Landais et al., 2013; this study). c: EDC ΔT_{site} (dark

504 green) and ΔT_{source} (green) reconstructions. d: EDC CH_4 (Loulergue et al., 2008). e: $\delta^{18}O_{calcite}$ from East Asian
505 speleothems in red (Cheng et al., 2016) and EDC $\delta^{18}O_{atm}$ in yellow (Extier et al., 2018). f: IRD percentage from site
506 ODP980 in black (McManus et al., 1999) and June 21st insolation at 65°N in grey (Laskar et al., 2004). g:
507 $\delta^{18}O_{planktonic}$ of core MD97-2120 (Pahnke et al., 2003). All ice core data are presented on the AICC2012 timescale,
508 the Δage estimate in AICC2012 between the gas and ice timescales being in excellent agreement (maximum
509 difference of 400 years) with the Δage obtained with the IGE firnification model presented here.

510

511 **5- Conclusions and perspectives**

512

513 We presented a high resolution record of $\delta^{15}N$ over Termination 3 on the Dome C ice core together
514 with a reconstruction of T_{site} and T_{source} from the combination of δD and d-excess on the same ice core.
515 $\delta^{15}N$ and T_{site} display early increases as soon as 256 and 253 ka while the δD record is mostly stable
516 until 251 ka. Based on a thorough data – firn model comparison, we demonstrated that impurity
517 concentration does not influence the $\delta^{15}N$ signal over Termination 3 and that the major part of the
518 $\delta^{15}N$ increase from 256 ka to the end of Termination 3 should better be related (directly or indirectly
519 through accumulation) to local temperature. It follows from this multiproxy analysis that the Antarctic
520 temperature increase over the first phase of Termination 3 is stronger than inferred from δD only.

521 Using a comparison with other climatic archives as well as indication for the timing of Weak
522 Monsoon Intervals in the EDC ice core and change in the low latitude water cycle through the $\delta^{18}O_{atm}$
523 proxy, we confirm a sequence of events suggested by Cheng et al. (2009): the two phases of Antarctic
524 temperature increase over Termination 3 are related to Heinrich like events with a bipolar seesaw
525 mechanism at play. The first phase occurs during a minimum of summer Northern Hemisphere
526 insolation with the bipolar seesaw associated with Heinrich like events being the major explanation
527 for Antarctic temperature increase while the second phase is associated with both Heinrich like event
528 and increase in summer Northern Hemisphere insolation. This contrasts with the two younger
529 terminations when the first Antarctic warming phase is in phase with increased in summer insolation
530 at 65°N.

531 This study confirms that using δD from the EDC ice core for reconstructing temperature evolution
532 should be done carefully. Indeed, millennial scale events can induce synchronous cooling of source and

533 site temperatures resulting in a stable δD . Multiproxy studies like the one performed here are thus
534 desirable and should be applied to other terminations such as Termination 4 associated with a strong
535 millennial variability at the end of MIS 10. This study opens perspective for deciphering the role of
536 orbital forcing and millennial variability in the onset and amplitude of a deglaciation.

537

538 **Acknowledgments**

539

540 The research leading to these results has received funding from the European Research Council
541 under the European Union's Seventh Framework Programme (FP7/2007-2013) / RC agreement
542 number 306045. It was also received funding from INSU/CNRS LEFE project NEVE-CLIMAT. Finally, this
543 work is a contribution to the European Project for Ice Coring in Antarctica (EPICA).

544

545 **References**

546

547 Barker, S., Diz, P., Vautravers, M.J., Pike, J., Knorr, G., Hall, I.R., Broecker, W.S., 2009. Interhemispheric
548 Atlantic seesaw response during the last deglaciation. *Nature* 457, 1097–1102.

549 Bazin, L., Landais, A., Lemieux-Dudon, B., Toyé Mahamadou Kele, H., Veres, D., Parrenin, F., Martinerie,
550 P., Ritz, C., Capron, E., Lipenkov, V., Loutre, M.-F., Raynaud, D., Vinther, B., Svensson, A.,
551 Rasmussen, S.O., Severinghaus, M., Blunier, T., Leuenberger, M., Fischer, H., Masson-Delmotte,
552 V., Chappellaz, J., Wolff, E., 2013. An optimized multi-proxy, multi-site Antarctic ice and gas orbital
553 chronology (AICC2012): 120-800 ka. *Clim. Past* 9, 1715–1731.

554 Bender, M.L., Sowers, T., Labeyrie, L., 1994. The Dole effect and its variations during the last 130,000
555 years as measured in the Vostok ice core. *Global Biogeochem. Cycles* 8, 363–376.

556 Bereiter, B., Eggleston, S., Schmitt, J., Nehrbass-Ahles, C., Stocker, T. F., Fischer, H., Kipfstuhl, S.,
557 Chappellaz, J., 2015. Revision of the EPICA Dome C CO₂ record from 800 to 600 kyr before present.
558 *Geophysical Research Letters* 42, 542–549.

559 Bernache-Assollant, D., 2005. Frittage : aspects physico-chimiques Partie 2 : frittage en phase liquide.

560 Bintanja, R., van de Wal, R.S.W., Oerlemans, J., 2005. Modelled atmospheric temperatures and global
561 sea levels over the past million years. *Nature* 437, 125–128.

562 Blunier, T. and Brook, E.J., 2001. Timing of millennial-scale climate change in Antarctica and Greenland
563 during the last glacial period. *Science* 291 (5501), 109–112.

564 Bréant, C., Martinerie, P., Orsi, A., Laurent, A., Landais, A., 2017. Modelling firn thickness evolution
565 during the last deglaciation: constraints on sensitivity to temperature and impurities. *Clim. Past*
566 13(7), 833–853.

567 Brook, E.J., Harder, S., Severinghaus, J., Steig, E.J., Sucher, C.M., 2000. On the origin and timing of rapid
568 changes in atmospheric methane during the Last Glacial Period. *Global Biogeochemical Cycles* 14
569 (2), 559–572.

570 Caillon, N., Severinghaus, J.P., Jouzel, J., Barnola, J.M., Kang, J., Lipenkov, V.Y., 2003. Timing of
571 atmospheric CO₂ and Antarctic temperature changes across Termination III. *Science* 299, 1728–
572 1731.

573 Capron, E., Landais, A., Lemieux-Dudon, B., Schilt, A., Masson-Delmotte, V., Buiron, D., Chappellaz, J.,
574 Dahl-Jensen, D., Johnsen, S., Leuenberger, M., Loulergue, L., Oerter, H., 2010. Synchronising EDML
575 and NorthGRIP ice cores using $\delta^{18}\text{O}$ of atmospheric oxygen ($\delta^{18}\text{O}_{\text{atm}}$) and CH₄ measurements over
576 MIS5 (80–123 kyr). *Quat. Sci. Rev.* 29, 222–234.

577 Capron, E., Landais, A., Buiron, D., Cauquoin, A., Chappellaz, J., Debret, M., Jouzel, J., Leuenberger, M.,
578 Martinerie, P., Masson-Delmotte, V., Mulvaney, R., Parrenin, F., Prié, F., 2013. Glacial–interglacial
579 dynamics of Antarctic firn columns: comparison between simulations and ice core air- $\delta^{15}\text{N}$
580 measurements. *Clim. Past* 9, 983–999.

581 Ciais, P. and Jouzel, J. 1994. Deuterium and oxygen 18 in precipitation: Isotopic model, including mixed
582 cloud processes. *Journal of Geophysical Research: Atmospheres* 99, 16793-16803

583 Cheng, H., Edwards, R. L., Broecker, W. S., Denton, G. H., Kong, X., Wang, Y., . . . Wang, X. (2009). Ice
584 Age Terminations. *Science*, 326(5950), 248-252. doi:10.1126/science.1177840

585 Cheng, H., Edwards, R.L., Sinha, A., Spötl, C., Yi, L., Chen, S., Kelly, M., Kathayat, G., Wang, X., Li, X.,
586 Kong, X., Wang, Y., Ning, Y., Zhang, H., 2016. The Asian monsoon over the past 640,000 years and
587 ice age terminations. *Nature* 534, 640–646.

588 Chiang, J.C.H., Bitz, C.M., 2005. Influence of high latitude ice cover on the marine Intertropical
589 Convergence Zone. *Clim. Dyn.* 25, 477–496.

590 Denton, G.H., Anderson, R.F., Toggweiler, J.R., Edwards, R.L., Schaefer, J.M., Putnam, A.E., 2010. The
591 last glacial termination. *Science* 328, 1652–1656.

592 Dreyfus, G.B., Jouzel, J., Bender, M.L., Landais, A., Masson-Delmotte, V., Leuenberger, M., 2010. Firn
593 processes and $\delta^{15}\text{N}$: potential for a gas-phase climate proxy. *Quat. Sci. Rev.* 29, 28–42.

594 Dütsch, M., Pfahl, S., Sodemann, H., 2017. The impact of nonequilibrium and equilibrium fractionation
595 on two different deuterium excess definitions. *Journal of Geophysical Research: Atmospheres*
596 122, 12732–12746.

597 EPICA Community Members, 2004. Eight glacial cycles from an Antarctic ice core. *Nature* 429, 623–
598 628.

599 EPICA Community Members, 2006. One-to-one coupling of glacial climate variability in Greenland and
600 Antarctica. *Nature* 444, 195–198.

601 Extier, T., Landais, A., Bréant, C., Prié, F., Bazin, L., Dreyfus, G., Roche, D.M., Leuenberger, M., 2018. On
602 the use of $\delta^{18}\text{O}_{\text{atm}}$ for ice core dating. *Quat. Sci. Rev.* 185, 244–257.

603 Fudge, T.J., Markle, B.R., Cuffey, K.M., Buizert, C., Taylor, K.C., Steig, E.J., Waddington, E.D., Conway,
604 H., Koutnik, M., 2016. Variable relationship between accumulation and temperature in West
605 Antarctica for the past 31,000 years. *Geophys. Res. Lett.* 43, 3795–3803.

606 Freitag, J., Kipfstuhl, S., Laepple, T., Wilhelms, F., 2013. Impurity-controlled densification: a new model
607 for stratified polar firn. *Journal of Glaciology* 59 (218), 1163–1169.

608 Gat, J.R., Matsui, E., 1991. Atmospheric water balance in the Amazon basin: an isotopic
609 evapotranspiration model. *J. Geophys. Res.* 96, 13179–13188.

610 Grachev, A.M. Severinghaus, J.P., 2003. Determining the thermal diffusion factor for Ar-40/Ar-36 in air
611 to aid paleoreconstruction of abrupt climate change. *J. Phys. Chem.* 107, 4636–4642.

612 Hodell, D.A., Channell, J.E.T., Curtis, J.H., Romero, O.E., Röhl, U., 2008. Onset of “Hudson Strait”
613 Heinrich events in the eastern North Atlantic at the end of the middle Pleistocene transition (~640
614 ka)? *Paleoceanography* 23, PA4218.

615 Hörhold, M.W., Laepple, T., Freitag, J., Bigler, M., Fischer, H., Kipfstuhl, S., 2012. On the impact of
616 impurities on the densification of polar firn. *Earth Planet. Sc. Lett.* 325, 93–99.

617 Huybers, P., 2007. Glacial variability over the last two million years: an extended depth-derived
618 agemodel, continuous obliquity pacing, and the Pleistocene progression. *Quat. Sci. Rev.* 26(1-2),
619 37–55.

620 Jiang, X., Kong, X., Wang, Y., Cheng, H., Wu, J., & Chen, S., 2010. Orbital-and millennial-scale variability
621 of the Asian monsoon during MIS8 from Sanbao Cave at Mount Shennongjia, central China.
622 *Chinese science bulletin* 55 (11), 1041–1046.

623 Jouzel, J., and Merlivat, L., 1984. Deuterium and oxygen-18 in precipitation: Modeling of the isotopic
624 effects during snow formation. *J. Geophys. Res.* 89 (D7), 11749–11757.

625 Jouzel, J., Vimeux, F., Caillon, N., Delaygue, G., Hoffmann, G., Masson-Delmotte, V., Parrenin, F., 2003.
626 Magnitude of isotope/temperature scaling for interpretation of central Antarctic ice cores. *J.*
627 *Geophys. Res.* 108 (D12), 4361.

628 Jouzel, J., Masson-Delmotte, V., Cattani, O., Dreyfus, G., Falourd, S., Hoffmann, G., Minster, B., Nouet,
629 J., Barnola, J.M., Chappellaz, J., Fischer, H., Gallet, J.C., Johnsen, S., Leuenberger, M., Loulergue,
630 L., Luethi, D., Oerter, H., Parrenin, F., Raisbeck, G., Raynaud, D., Schilt, A., Schwander, J., Selmo,
631 E., Souchez, R., Spahni, R., Stauffer, B., Steffensen, J.P., Stenni, B., Stocker, T.F., Tison, J.L., Werner,
632 M., Wolff, E.W., 2007. Orbital and millennial Antarctic climate variability over the past 800,000
633 years. *Science* 317, 793–796.

634 Lambert, F., Bigler, M., Steffensen, J.P., Hutterli, M., Fischer, H., 2012. Centennial mineral dust
635 variability in high-resolution ice core data from Dome C, Antarctica. *Clim. Past* 8, 609–623.

636 Landais, A., Barnola, J. M., Kawamura, K., Caillon, N., Delmotte, M., Van Ommen, T., Dreyfus, G., Jouzel,
637 J., Masson-Delmotte, V., Minster, B., Freitag, J., Leuenberger, M., Schwander, J., Huber, C.,
638 Etheridge, D., Morgan, V., 2006. Firn-air $\delta^{15}\text{N}$ in modern polar sites and glacial–interglacial ice: a
639 model-data mismatch during glacial periods in Antarctica? *Quat. Sci. Rev.* 25, 49–62.

640 Landais, A., Dreyfus, G., Capron, E., Masson-Delmotte, V., Sanchez-Goñi, M.F., Desprat, S., Hoffmann,
641 G., Jouzel, J., Leuenberger, M., Johnsen, S., 2010. What drives the millennial and orbital variations
642 of $\delta^{18}\text{O}_{\text{atm}}$? *Quat. Sci. Rev.* 29, 235–246.

643 Landais, A., Dreyfus, G., Capron, E., Jouzel, J., Masson-Delmotte, V., Roche, D.M., Prié, F., Caillon, N.,
644 Chappellaz, J., Leuenberger, M., Lourantou, A., Parrenin, F., Raynaud, D., Teste, G., 2013. Two-
645 phase change in CO_2 , Antarctic temperature and global climate during Termination II. *Nat. Geosci.*
646 6, 1062–1065.

647 Landais, A., Masson-Delmotte, V., Stenni, B., Selmo, E., Roche, D.M., Jouzel, J., Lambert, F., Guillevic,
648 M., Bazin, L., Arzel, O., Vinther, B., Gkinis, V., Popp, T., 2015. A review of the bipolar seesaw from
649 synchronized and high resolution ice core water stable isotope records from Greenland and East
650 Antarctica. *Quat. Sci. Rev.* 114, 18–32.

651 Laskar, J., Robutel, P., Joutel, F., Gastineau, M., Correia, A.C.M., Levrard, B., 2004. A long-term
652 numerical solution for the insolation quantities of the Earth. *Astron. Astrophys* 428, 261–285.

653 Louergue, L., Schilt, A., Spahni, R., Masson-Delmotte, V., Blunier, T., Lemieux, B., Barnola, J.-M.,
654 Raynaud, D., Stocker, T.F., Chappellaz, J., 2008. Orbital and millennial-scale features of
655 atmospheric CH_4 over the past 800,000 years. *Nature* 453, 383–386.

656 Lüthi, D., Le Floch, M., Bereiter, B., Blunier, T., Barnola, J.-M., Siegenthaler, U., Raynaud, D., Jouzel, J.,
657 Fischer, H., Kawamura, K., Stocker, T.F., 2008. High-resolution carbon dioxide concentration
658 record 650,000–800,000 years before present. *Nature* 453, 379–382.

659 Markle, B.R., Steig, E.J., Buizert, C., Schoenemann, S.W., Bitz, C.M., Fudge, T.J., Pedro, J.B., Ding, Q.,
660 Jones, T.R., White, J.W.C, Todd, S., 2016. Global atmospheric teleconnections during Dansgaard-
661 Oeschger events. *Nat. Geosci.* 10, 36–40.

662 Masson-Delmotte, V., Stenni, B., Blunier, T., Cattani, O., Chappellaz, J., Cheng, H., Dreyfus, G.,
663 Edwards, R. L., Falourd, S., Govin, A., Kawamura, K., Johnsen, S. J., Jouzel, J., Landais, A., Lemieux-
664 Dudon, B., Lourantou, A., Marshall, G., Minster, B., Mudelsee, M., Pol, K., Röthlisberger, R., Selmo,
665 E., Waelbroeck, C., 2010. Abrupt change of Antarctic moisture origin at the end of Termination II.
666 P. Natl. Acad. Sci. USA, 107, 12091–12094.

667 McManus, J.F., Oppo, D.W., Cullen, J.L., 1999. A 0.5 million-year record of millennial scale climate
668 variability in the North Atlantic. Science 283, 971–975.

669 McManus, J.F., Francois, R., Gherardi, J.M., Keigwin, L.D., Brown-Leger, S., 2004. Collapse and rapid
670 resumption of Atlantic meridional circulation linked to deglacial climate changes. Nature 428,
671 834–837.

672 Merlivat L. and Jouzel J., 1979. Global climatic interpretation of the deuterium-oxygen–18 relationship
673 or precipitation. J. Geophys. Res. 84, 5029–5033.

674 Meyer, H., Schönicke, L., Wand, U., Hubberten, H.-W., Friedrichsen, H., 2000. Isotope studies of
675 hydrogen and oxygen in ground ice-experiences with the equilibration technique. Isot. Environ.
676 Health Stud. 36 (2), 133–149.

677 Milankovitch, M., 1941. History of radiation on the Earth and its use for the problem of the ice ages. K.
678 Serb. Akad. Beogr.

679 Obrochta, S.P., Crowley, T.J., Channell, J.E., Hodell, D.A., Baker, P.A., Seki, A., Yokoyama, Y., 2014.
680 Climate variability and ice-sheet dynamics during the last three glaciations. Earth and Planetary
681 Science Letters 406, 198–212.

682 Past Interglacials Working Group of PAGES, 2016. Interglacials of the last 800,000 years. Reviews of
683 Geophysics 54, 162–219.

684 Pahnke, K., Zahn, R., Elderfield, H., Schulz, M., 2003. 340,000 year centennial-scale marine record of
685 Southern Hemisphere climatic oscillation. Science 301, 948–952.

686 Paillard, D., 1998. The timing of Pleistocene glaciations from a simple multiple-state climate model.
687 Nature 391, 378–381.

688 Paillard, D., Parrenin, F., 2004. The Antarctic ice sheet and the triggering of deglaciations. *Earth and*
689 *Planetary Science Letters* 227, 263–271.

690 Parrenin, F., Remy, F., Ritz, C., Siegert, M., Jouzel, J., 2004. New modelling of the Vostok ice flow
691 line and implication for the glaciological chronology of the Vostok ice core. *J. Geophys. Res.*,
692 109, D20102.

693 Parrenin, F., Barnola, J.-M., Beer, J., Blunier, T., Castellano, E., Chappellaz, J., Dreyfus, G., Fischer, H.,
694 Fujita, S., Jouzel, J., Kawamura, K., Lemieux-Dudon, B., Loulergue, L., Masson-Delmotte, V., Narcisi,
695 B., Petit, J.-R., Raisbeck, G., Raynaud, D., Ruth, U., Schwander, J., Severi, M., Spahni, R., Steffensen,
696 J. P., Svensson, A., Udisti, R., Waelbroeck, C., Wolff, E., 2007. The EDC3 chronology for the EPICA
697 Dome C ice core. *Clim. Past* 3, 485–497.

698 Parrenin, F., Barker, S., Blunier, T., Chappellaz, J., Jouzel, J., Landais, A., Masson-Delmotte, V.,
699 Schwander, J., Veres, D., 2012. On the gas-ice depth difference (Δ depth) along the EPICA Dome C
700 ice core. *Clim. Past* 8, 1239–1255.

701 Parrenin, F., Masson-Delmotte, V., Kohler, P., Raynaud, D., Paillard, D., Schwander, J., Barbante, C.,
702 Landais, A., Wegner, A., Jouzel, J., 2013. Synchronous Change of Atmospheric CO₂ and Antarctic
703 Temperature During the Last Deglacial Warming. *Science* 339, 1060–1063.

704 Pedro, J.B., Rasmussen, S.O., van Ommen, T.D., 2012. Tightened constraints on the time-lag between
705 Antarctic temperature and CO₂ during the last deglaciation. *Clim. Past* 8, 1213–1221.

706 Pedro, J.B., Jochum, M., Buizert, C., He, F., Barker, S., Rasmussen, S.O., 2018. Beyond the bipolar
707 seesaw: toward a process understanding of interhemispheric coupling. *Quat. Sci. Rev.* 192, 27–
708 46.

709 Pérez-Mejías, C., Moreno, A., Sancho, C., Bartolomé, M., Stoll, H., Cacho, I., Cheng, H., Edwards, R.L.,
710 2017. Abrupt climate changes during Termination III in Southern Europe. *Proceedings of the*
711 *National Academy of Sciences* 114, 10047–10052.

712 Reutenauer, C., Landais, A., Blunier, T., Bréant, C., Kageyama, M., Woillez, M.-N., Risi, C., Mariotti, V.,
713 Braconnot, P., 2015. Quantifying molecular oxygen isotope variations during a Heinrich stadial.
714 *Clim. Past* 11, 1527–1551.

715 Rhodes, R.H., Brook, E.J., Chiang J., Blunier, T., Maselli, O., McConnel, J.R., Romanini, D., Severinghaus,
716 J., 2015. Enhanced tropical methane production in response to iceberg discharge in the North
717 Atlantic. *Science* 348 (6238), 1016–1019.

718 Röhling, E.J., Foster, G.L., Grant, K.M., Marino, G., Roberts, A.P., Tamisiea, M.E., Williams, F., 2014. Sea-
719 level and deep-sea-temperature variability over the past 5.3 million years. *Nature* 508, 477–482.

720 Röthlisberger, R., Mudelsee, M., Bigler, M., de Angelis, M., Fisher, H., Hansson, M., Lambert, F.,
721 Masson-Delmotte, V., Sime, L., Udisti, R., Wolff, E.W., 2008. The Southern Hemisphere at glacial
722 terminations: insights from the Dome C ice core. *Clim. Past* 4, 345–356.

723 Seltzer, A.M., Buizert, C., Baggenstos, D., Brook, E.J., Ahn, J., Yang, J.-W., Severinghaus, J.P., 2017. Does
724 $\delta^{18}\text{O}$ of O_2 record meridional shifts in tropical rainfall? *Clim. Past* 13, 1323–1338.

725 Severinghaus, J.P., Sowerst, T. & Alley, R.B., 1998. Timing of abrupt climate change at the end of the
726 Younger Dryas interval from thermally fractionated gases in polar ice. *Nature* 39, 141–146.

727 Severinghaus, J.P., Beaudette, R., Headly, M.A., Taylor, K., Brook, E.J., 2009. Oxygen-18 of O_2 records
728 the impact of abrupt climate change on the terrestrial biosphere. *Science* 324, 1431–1434.

729 Sowers, T., Bender, M.L., Raynaud, D., Korotkevich, Y.S., 1992. ^{15}N of N_2 in air trapped in polar ice: a
730 tracer of gas transport in the firn and a possible constraint on ice age–gas age differences. *Journal*
731 *of Geophysical Research* 97, 15,683–15,697.

732 Spratt, R.M., & Lisiecki, L.E., 2016. A Late Pleistocene sea level stack. *Clim. Past* 12, 1079–1092.

733 Stenni, B., Masson-Delmotte, V., Johnsen, S., Jouzel, J., Longinelli, A., Monnin, E., Röthlisberger, R.,
734 Selmo, E., 2001. An oceanic cold reversal during the last deglaciation. *Science* 293, 2074–2077.

735 Stenni, B., Masson-Delmotte, V., Selmo, E., Oerter, H., Meyer, H., Röthlisberger, R., Jouzel, J., Cattani,
736 O., Falourd, S., Fisher, H., Hoffmann, G., Lacumin, P., Johnsen, S.J., Minster, B., Udisti, R., 2010.

737 The deuterium excess records of EPICA Dome C and Maud Land ice cores (East Antarctica). *Quat.*
738 *Sci. Rev.* 29, 146–159.

739 Stocker, T.F., Johnsen, S.J., 2003. A minimum thermodynamic model for the bipolar seesaw.
740 *Paleoceanography* 18, 1087.

741 Touzeau, A., Landais, A., Stenni, B., Uemura, R., Fukui, K., Fujita, S., 2016. Acquisition of isotopic
742 composition for surface snow in East Antarctica and the links to climatic parameters. *Cryosphere*,
743 10 (2), 837–852.

744 Tzedakis, P.C., Crucifix, M., Mitsui, T., & Wolff, E.W., 2017. A simple rule to determine which insolation
745 cycles lead to interglacials. *Nature* 542, 427–432.

746 Uemura, R., Masson-Delmotte, V., Jouzel, J., Landais, A., Motoyama, H., Stenni, B., 2012. Ranges of
747 moisture-source temperature estimated from Antarctic ice cores stable isotope records over
748 glacial–interglacial cycles. *Clim. Past* 8 (3), 1109–1125.

749 Uemura, R., Motoyama, H., Masson-Delmotte, V., Jouzel, J., Kawamura, K., Goto-Azuma, K., Fujita, S.,
750 Kuramoto, T., Hirabayashi, M., Miyake, T., Ohno, H., Abe-Ouchi, A., Iizuka, Y., Horikawa, S.,
751 Igarashi, M., Suzuki, K., Suzuki, T., Fujii, Y., 2018. Asynchrony between Antarctic temperature and
752 CO₂ associated with obliquity over the past 720,000 years. *Nat. Comm.* 9 (961).

753 Veres, D., Bazin, L., Landais, A., Toyé Mahamadou Kele, H., Lemieux-Dudon, B., Parrenin, F., Martinerie,
754 P., Blayo, E., Blunier, T., Capron, E., Chappellaz, J., Rasmussen, S.O., Severi, M., Svensson, A.,
755 Vinther, B., Wolff, E.W., 2013. The Antarctic ice core chronology (AICC2012): an optimized multi-
756 parameter and multi-site dating approach for the last 120 thousand years. *Clim. Past* 9, 1733–
757 1748.

758 Vimeux, F., Masson, V., Jouzel, J., Stievenard, M., Petit, J.R., 1999. Glacial–interglacial changes in ocean
759 surface conditions in the Southern Hemisphere. *Nature* 398, 410–413.

760 Vimeux, F., Masson, V., Jouzel, J., Petit, J.R., Steig, E.J., Stievenard, M., Vaikmae, R., White, J.W.C., 2001.
761 Holocene hydrological cycle changes in the southern hemisphere documented in East Antarctic
762 deuterium excess records. *Clim. Dyn.* 17, 503–513.

763 Wang, Y.J., Cheng, H., Edwards, R.L., Kong, X., Shao, X., Chen, S., Wu, J., Jiang, X., Wang, X., An, Z., 2008.
764 Millennial- and orbital-scale changes in the East Asian monsoon over the past 224,000 years.
765 Nature 451, 1090–1093.

766 Watanabe, O., Jouzel, J., Johnsen, S., Parrenin, F., Shoji, H., Yoshida, N., 2003. Homogeneous climate
767 variability across East Antarctica over the past three glacial cycles. Nature 422, 509–512.

768 Wilkinson, D.S. and Ashby, M.F., 1975. Pressure sintering by power law creep. Acta Metall. 23, 1277–
769 1285.

770 Wolff, E.W., Fischer, H., Rothlisberger, R., 2009. Glacial terminations as southern warmings without
771 northern control. Nature Geoscience 2, 206–209.

772 Yin, Q. Z. and Berger, A., 2012. Individual contribution of insolation and CO₂ to the interglacial climates
773 of the past 800,000 years. Clim. Dyn. 38, 709–724.

774 Yu, Z., Loisel, J., Turetsky, M.R., Cai, S., Zhao, Y., Frohking, S., MacDonald, G.M., Bubier, J.L., 2013.
775 Evidence for elevated emissions from high-latitude wetlands contributing to high atmospheric CH₄
776 concentration in the early Holocene. Global Biogeochem. Cycles 27, 131–140.

777 Zhang, H., Griffiths, M.L., Huang, J., Cai, Y., Wang, C., Zhang, F., Cheng, H., Ning, Y., Hu, C., Xie, S., 2016.
778 Antarctic link with East Asian summer monsoon variability during the Heinrich Stadial–Bølling
779 interstadial transition. Earth Planet. Sci. Lett. 453, 243–251.